Polyhedron 170 (2019) 287–293

Contents lists available at ScienceDirect

Polyhedron

journal homepage: www.elsevier.com/locate/poly

A new ladder-type dichloro(2,2-dimethyl-1,3-diaminopropane) copper complex: Synthesis, structural studies and selective sensing behavior towards a ketone molecule

Mohammad Azam [a,*], Saud I. Al-Resayes [a], Mahboob Alam [b], Agata Trzesowska-Kruszynska [c], Rafal Kruszynski [c], Mohammed Rafiq H. Siddiqui [a]

[a] Department of Chemistry, College of Science, King Saud University, P.O. Box 2455, Riyadh 11451, Saudi Arabia
[b] Division of Chemistry and Biotechnology, Dongguk University, 123 Dongdae-ro, Gyeongju, Republic of Korea
[c] Institute of General and Ecological Chemistry, Lodz University of Technology, Zeromskiego 116, 90-924 Lodz, Poland

ARTICLE INFO

Article history:
Received 13 February 2019
Accepted 27 May 2019
Available online 10 June 2019

Keywords:
$Cu(dmpd)Cl_2$
Synthesis
Crystal structure
DFT studies
Fluorescence properties

ABSTRACT

A new coordination compound with the formula $[Cu(dmpd)Cl_2]$, where dmpd stands for 2,2-dimethyl-propane-1,3-diamine, was prepared and structurally characterised by elemental analyses, IR and UV/Vis spectroscopic studies. The single crystal X-ray crystallographic study revealed the copper cation to be six coordinated in the complex by two amine nitrogen atoms and four chloride ions. The copper atom adopts a distorted tetragonal bipyramidal geometry, with two bridging chloride ions located at the polyhedron apexes. Furthermore, to obtain insight into the structure, theoretical studies were performed. The complex exhibits a strong photoluminescence property in tetrahydrofuran and shows a strong sensing behaviour towards a ketone molecule, proving it to be a good candidate for sensing measurements.

1. Introduction

Literature reveals that the coordination behavior of diamines with a flexible framework leads to various conformations. However, the symmetry of the resulting structures mostly depends on the coordinated moieties and the nucleophilicity of the anion [1]. There are reports that propane-1,3-diamines have a greater coordination flexibility than ethylenediamines, and forms coordination compounds with unique structures upon interaction with metal ions [2]. 2,2-Dimethyl-1,3-propanediamine, abbreviated in this paper as dmpd, is the most versatile bidentate ligand among the propanediamines [2–6], and coordinates to metal ions forming a six-membered chelate ring via the two nitrogen atoms [4,6].

In this paper, we discuss the preparation of a new copper complex with 2,2-dimethyl-1,3-diaminopropane (dmpd) as the building ligand and dichlorocuprate(II) as an inorganic anion in a 1:1 molar ratio. To the best of our knowledge, this is the first ever report on the synthesis of $Cu(dmpd)Cl_2$. However, earlier reports have shown the preparation of a copper complex by the reaction of dmpd with $CuCl_2$ in a 2:1 molar ratio [7]. The $[Cu(dmpd)Cl_2]$ complex has been structurally investigated by means of single crystal X-ray structure analysis together with IR and UV/Vis studies. Further, to get insight into the structural and electronic properties, time dependent (TD-DFT) measurements were carried out. Theoretical measurement results were consistent with the experimental findings. In addition, the photoluminescence properties and sensing behavior of the complex was investigated. The complex showed effective quenching properties towards a ketone molecule.

2. Experimental

All chemicals and solvents were commercially available and used as received. The ligand used in the synthesis of $[Cu(dmpd)Cl_2]$ was prepared as described earlier [8]. FT-IR spectra were recorded on a Perkin Elmer 621 spectrophotometer using KBr pellets. Elemental analyses (EA) for C, H and N were carried out on an Elementar Varrio EL analyzer. Fluorescence spectra were obtained on a RF-6000 spectrofluorometer.

2.1. Synthesis of the copper complex, $[Cu(dmpd)Cl_2]$

The copper complex was synthesized by the reaction of the ligand dmpd (0.50 mg, 0.145 mmol) [8] with $CuCl_2{\cdot}H_2O$ in a 1:1 stoichiometric ratio in methanol. The reaction mixture was stirred

* Corresponding author. Fax: +966 1 4675982.
E-mail addresses: mhashim@ksu.edu.sa, azam_res@yahoo.com (M. Azam).

https://doi.org/10.1016/j.poly.2019.05.053
0277-5387/

for 5 h, leading to the formation of small sediment which was separated out, and then the filtrate was allowed to evaporate at room temperature. After a few days, blue colored prismatic crystals of [Cu(dmpd)Cl_2] were obtained. The formation of the complex was supposed to be due to various factors mentioned in literature [9,10].

Color: Blue; Elemental analyses (Calculated) C, 25.38; H, 5.96; N, 11.84; (Found): C, 25.36; H, 5.93; N, 11.81; IR (KBr, cm^{-1}) 773 ν(–CH_2), 910 ν(–NH_2)

2.2. Crystal structure determination

X-ray diffraction studies for a blue prismatic crystal of the catena-((μ_3-chloro)-chloro-(2,2-dimethylpropane-1,3-diamine-N, N′)-copper(II)) complex were carried out on a Rigaku Synergy Dualflex automatic diffractometer equipped with a Pilatus 300 K detector (λ(Mo Kα) = 0.71073 Å, monochromated) via the ω scan mode. A summary of the data collection and refinement details are given in Table 1. All calculations were performed using the SHELXS [11], SHELXL [12] and SHELXTL [13] programs. Atomic scattering factors were taken from the International Tables for Crystallography [14]. Selected interatomic bond distances are summarized in Table 2 and intermolecular interactions in Table 3.

2.3. Computational details

The [Cu(dmpd)Cl_2] complex was investigated using density functional theory with Gaussian software [15], and the crystallographic structure fragment [Cu(dmpd)Cl_2] was used as the starting geometry for the optimization procedures. The functional B3LYP, where B3 and LYP represent the functional correlation of the three-parameter Becke [16] and Lee-Yang-Parr hybrid [17], was used together with the 6-311G(d,p) basis set for all atoms. However, the basis set of LAN2DZ [18–21] for the Cu atom was also used to optimize and compute the electronic transitions of the complex to better reconcile the accuracy and computational cost. Other parameters of the compound were also calculated by combining the basis sets 6-311G(d,p) and LAN2DZ. The studied copper complex has an odd number of electrons, i.e. an open-shell system. An unrestricted calculation was therefore applied where independent consideration was given to the two spin populations. The IR frequencies were calculated in harmonic approximation for the optimized molecule and it was found that the optimized geometry on the potential energy surface was at a minima and real values of the theoretical IR frequencies were ascertained. The electronic properties and spectra were calculated using the polarizable continuum model (PCM) in EtOH with the mixed basis set. Percentage contributions of the molecular orbitals to the electronic transitions were collected by GaussSum [22].

Table 1
Crystal and structure refinement data of compound.

Empirical formula	$C_5H_{14}Cl_2CuN_2$
Formula weight	236.62
Crystal system, space group	monoclinic, $P2_1/n$ (No.14)
Unit cell dimensions [Å, °]	
a	12.5467(6)
b	5.8858(2)
c	13.4231(6)
β	115.794(6)
V [Å^3]	892.50(8)
Z	4,
Calculated density [Mg/m^3]	1.761
F(0 0 0)	484
Crystal size [mm]	0.112, 0.109, 0.104
θ range for data collection [°]	3.607 to 32.142
Index ranges	$-18 \le h \le 18$, $-8 \le k \le 8$, $-19 \le l \le 19$
Reflections collected/unique	18 797/2732 [R_{int} = 0.0419]
Completeness [%]	99.8 (to θ = 25°)
Data/restraints/parameters	2732/0/109
Goodness-of-fit (GoF) on F^2	1.070
Final R indices [$I > 2\sigma(I)$]	$R1$ = 0.0197, $wR2$ = 0.0523
R indices (all data)	$R1$ = 0.0215, $wR2$ = 0.0530
Largest difference peak and hole [e Å^{-3}]	0.525 and −0.746

Table 2
Selected structural data of compound **1** [Å, °].

Cu1–N2	2.0044(10)
Cu1–N1	2.0179(10)
Cu1–Cl2	2.3030(3)
Cu1–Cl1	2.3278(3)
Cu1–Cl1^{i}	2.7690(3)
Cu1–Cl1^{ii}	3.1371(3)
N2–Cu1–N1	93.36(4)
N2–Cu1–Cl2	91.17(3)
N1–Cu1–Cl2	174.61(3)
N2–Cu1–Cl1	170.84(3)
N1–Cu1–Cl1	84.59(3)
Cl2–Cu1–Cl1	90.486(12)
N2–Cu1–Cl1^{i}	89.44(3)
N1–Cu1–Cl1^{i}	89.55(3)
Cl2–Cu1–Cl1^{i}	93.428(9)
Cl1–Cu1–Cl1^{i}	99.463(10)
N2–Cu1–Cl1^{ii}	81.24(3)
N1–Cu1–Cl1^{ii}	89.13(3)
Cl2–Cu1–Cl1^{ii}	88.670(9)
Cl1–Cu1–Cl1^{ii}	89.785(9)
Cl1^{i}–Cu1–Cl1^{ii}	170.491(12)
Cu1–Cl1–Cu1^{ii}	89.637(9)

Symmetry transformations used to generate equivalent atoms: (i) $-x + 3/2, y + 1/2, -z + 3/2$; (ii) $-x + 3/2, y - 1/2, -z + 3/2$.

3. Results and discussion

The asymmetric part of the [Cu(dmpd)Cl_2] unit cell (Fig. 1) consists of the 2,2-dimethylpropane-1,3-diamine ligand coordinating to the copper cation via two amine nitrogen atoms and two copper-coordinating chloride anions. All the atoms occupy general positions, however, the presence of a twofold screw axis going through the Cu1-Cl1 bond expands the monomeric [Cu($C_5H_{14}N_2$)Cl_2] units into a 1D polymeric chain (ladder-type) extending along the crystallographic [0 1 0] axis (Fig. 2). This form is distinctly different from that observed in bis(2,2-dimethylpropane-1,3-diamine)-dichloro-copper(II) tetrahydrate [23], in which the mononuclear molecule is observed and the metal to ligand stoichiometry is 1:2 (versus 1:1 existing in this studied compound). In (dmpd)$CuCl_2$, the copper cation is six-coordinated by two amine nitrogen atoms, and four chloride ions (two from the asymmetric unit and two from two neighbouring asymmetric units). The one chloride ion act as a monodentate ligand and the second one as a tridentate ligand bridging three copper cations. Thus, the copper atom adopts a distorted tetragonal bipyramid geometry [24] with the two bridging chloride ions located at the polyhedron apexes. Geometry distortion is caused by steric restrains imposed by the chelating organic ligand. The analysis of the coordination bonds lengths (Table 2) shows a strong Jahn–Teller distortion (tetragonal elongation), nevertheless the axial ligands are in bonding positions, which is confirmed by bond valences calculations. The bond valences were computed as $v_{ij} = \exp[(R_{ij} - d_{ij})/b]$ [25,26], where R_{ij} is the bond-valence parameter (in the formal sense R_{ij} can be considered as a parameter equal to the idealised single-bond length between i and j atoms for a given b value [27–29]) and b

Table 3
Hydrogen bonds geometry of compound **1** [Å, °]

D–H···A	d(D–H)	d(H···A)	d(D···A)	<(DHA)
N1–H1NA···Cl2^{ii}	0.853(16)	2.673(16)	3.4612(10)	154.4(14)
N1–H1NB···Cl2^{i}	0.859(18)	2.793(17)	3.6018(10)	157.6(14)
N1–H1NA···Cl1	0.853(16)	2.616(15)	2.9334(11)	103.4(11)
N2–H2NA···Cl1^{i}	0.855(17)	2.902(16)	3.4561(11)	124.2(12)
N2–H2NA···Cl2^{iv}	0.855(17)	2.648(16)	3.3720(11)	143.2(13)
N2–H2NB···Cl1^{v}	0.876(18)	2.769(18)	3.5706(11)	152.8(14)
N2–H2NB···Cl2	0.876(18)	2.805(17)	3.0838(11)	100.2(13)
C3–H3A···Cl2^{iii}	0.99	2.90	3.6001(12)	128.1
C4–H4A···Cl1^{i}	0.98	2.71	3.6773(12)	168.0

Symmetry transformations used to generate equivalent atoms: (i) $-x+3/2, y+1/2, -z+3/2$; (ii) $-x+3/2, y-1/2, -z+3/2$; (iii) $-x+1, -y+2, -z+1$; (iv) $-x+1, -y+1, -z+1$; (v) $x-1/2, -y+3/2, z-1/2$.

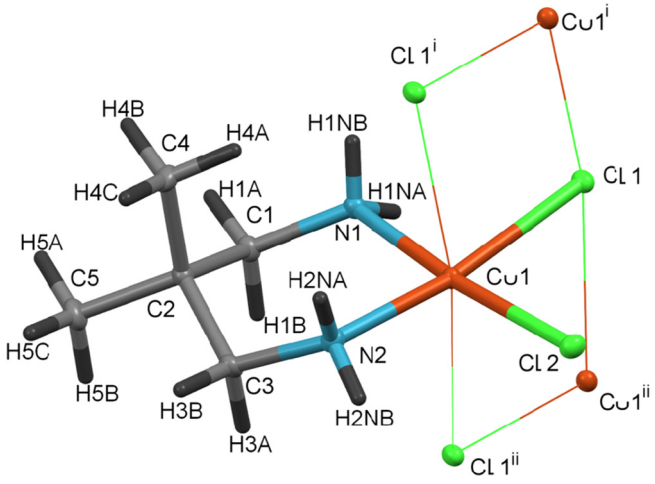

Fig. 1. The molecular structure plotted with 50% probability of the displacement ellipsoids. The bonds of symmetry generated atoms are indicated by thin lines. Symmetry codes are as in Table 1.

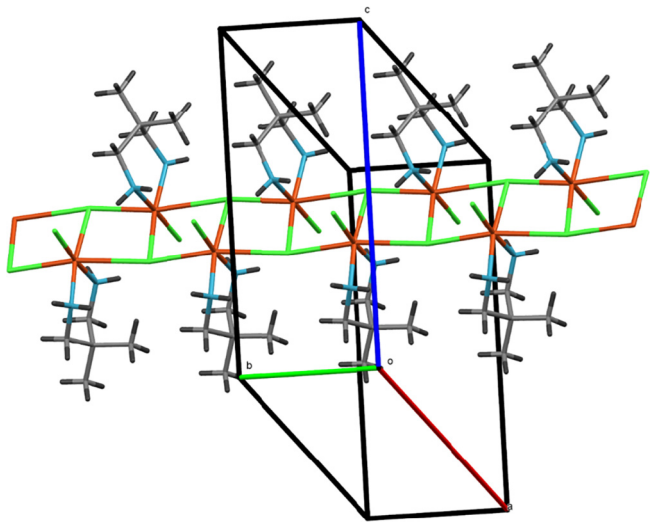

Fig. 2. Part of the molecular packing, showing the coordination polymer chain. The atom colours are as in Fig. 1.

was taken as 0.37 Å [7,30]. R_{Cu-N} and R_{Cu-Cl} were taken as 1.713 and 2.000 Å, respectively [31,32]. The computed bond valences show that all the coordination bonds with the basal donor atoms possess similar strengths (v_{Cu1-N1} = 0.439, v_{Cu1-N2} = 0.455, $v_{Cu1-Cl1}$ = 0.412, and $v_{Cu1-Cl2}$ = 0.441 v.u.) and the coordination bonds of the apical ligands are distinctly weaker, from one quarter to one tenth of the basal coordination bonds ($v_{Cu1-Cl1(i)}$ = 0.125 and 0.046 $v_{Cu1-Cl1(ii)}$ v.u.; symmetry codes as in Table 2). The total valence of the Cu^{2+} cation is 1.92 v.u, which is slightly smaller than the formal oxidation state of the copper ion, which proves that both apical chloride ligands forms coordination bonds with the copper cation. Multiple intramolecular N–H···Cl hydrogen bonds (Table 3) provide additional stabilisation to the formed polymeric chain. The intermolecular N2–H2NA···Cl2^{iv}, N2–H2NB···Cl1^{v} and C3–H3A···Cl2^{iii} interactions [33] interlink neighbouring chains to form a supramolecular net extending along crystallographic (1 0 –1) plane. The intermolecular N–H···Cl hydrogen bonds form a unitary graph set of the lowest degree, containing two $R_2^2(8)$ ring patterns [34].

The [Cu(dmpd)Cl_2] complex containing 2,2-dimethylpropane-1,3-diamine was properly improved in the gas phase using b3lyp/6-311G(d,p) and b3lyp/lanl2dz in order to compare the best optimized structure to the experimental results. Fig. S1 (Supplementary Information) represents atomic numbering scheme of the optimized structure of the metal complex. Important structural parameters of the [Cu(dmpd)Cl_2] complex are listed in Table S1, showing the acceptable results from both basis sets. To determine the consistency between the predicted and the experimental values, the largest differences in bond length and angle were taken into account for consideration. The largest difference between the experimental and predicted values (0.15 Å, b3lyp/6-311G(d,p); 9.2°, b3lyp/6-311G(d,p); 5.0° b3lyp/lanl2dz) were observed for the N_2–H_2N bond and the Cl1–Cu1–Cl_2 angle. The alternation of bond angles and length in the geometry of the B3LYP basis set is higher than observed in the experimental findings. However, deflection between the experimental and theoretical structural parameters is likely due to the intra and intermolecular interactions which are not taken into account in the crystalline phase calculations. Most of the complex computed parameters are related to the experimental values obtained from the single X-ray crystallography. To determine the long-range dispersion interactions, in particular for this complex with inter or intramolecular interactions, the complex was optimized using the B3LYP-D3 [35] basis set of dispersion corrections, where D3 denotes the Grimm correction. Multiwfn [36] and AIM programs [37] were used together to draw and explain the reduced density gradient (RDG) in order to represent a more intuitive understanding of the inter- and intramolecular attractions, graphically explained in Figs. S2 and S3 (Supplementary Information). The IR spectrum of the compound, illustrated in Fig. 3, includes strong bending vibrations due to $\beta_{(-NH2)}$ and $\beta_{(-CH2)}$ groups at 1579 and 1629 cm^{-1}, and a single band at 1415 cm^{-1} [38–40]. The unambiguous assignment for $\nu_{asy\ \&\ sym(NH)}$ and $\nu_{sym(CH)}$ vibrations were noted at 3430, 3274 and 2957 cm^{-1}, respectively [38–40]. The $\nu_{\rho(CH2)}$ and $\nu_{\rho(NH2)}$ vibrations were noted at 773 and 910 cm^{-1}, whereas the characteristic vibration due to $\nu_{\delta(CH2)}$ was found at 2850 cm^{-1} [38–40]. Individual

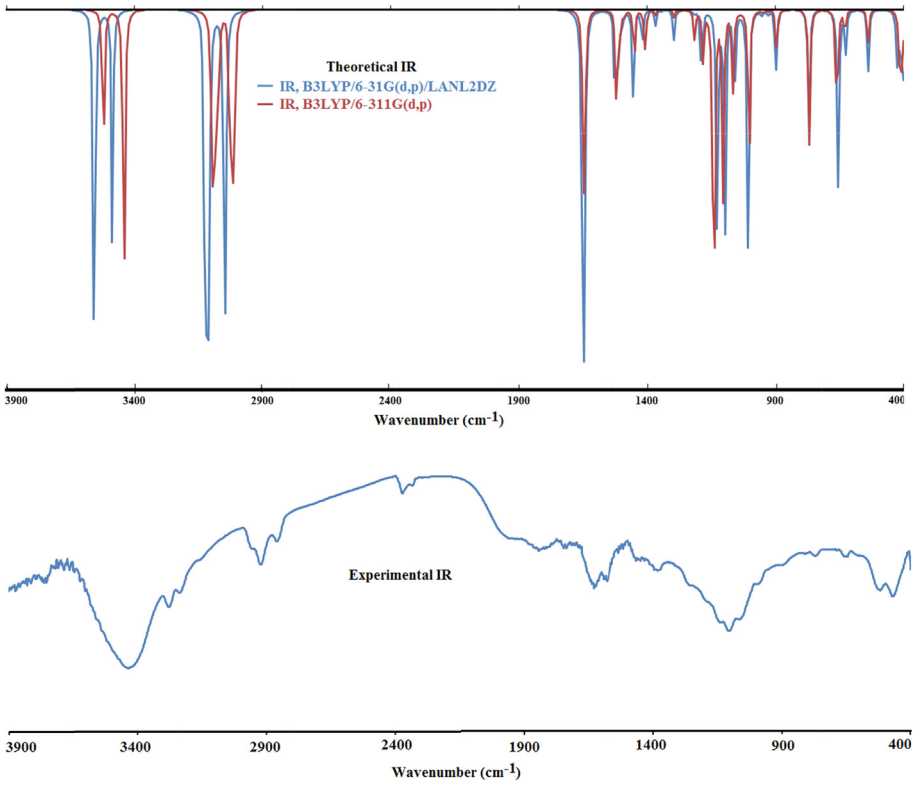

Fig. 3. Experimental and theoretical FTIR spectra.

band assignments observed in the experimental IR spectra, with the theoretical harmonic frequencies and IR intensities are shown in Table S2. The vibrational bands observed in the experimental findings were compared with their theoretical values, in both position and intensity, and the Harmonic IR frequencies were analogous to the experimental data using a scaling factor [41] (Table S2). However, the theoretical values proved to be more arbitrary compared to the experimental values, probably because of the negligence of anharmonicity calculations. This may also be due to carrying out the calculations in the gas phase, while the experimental values were recorded in the solid state. The possible vibrations due to the $-NH_2$ and $-CH_2$ group were symmetrical, asymmetrical stretching, scissors, balancing, movement and torsion (Table S2). The $-NH_2$ group vibrates asymmetrically and symmetrically at 3522 and 3442 cm^{-1}, respectively. The $-NH_2$ functionality displayed medium to strong absorption bands attributed to a scissoring vibration at 1650 and 1580 cm^{-1}. In addition, –CH stretching vibrations were noted at 3099, 3093, 3089, 3083 and 3011 cm^{-1}. Other typical bands in the experimental spectrum at 1580 and 1470 cm^{-1} [42] are ascribed to the symmetric in-plane deformation vibration (scissoring). The considerable deviation for hydrogenic stretching vibrations is marked between the experimental and theoretical frequencies. Scaling factors applied in the present analysis are given in Table S2 to correlate the theoretical vibrational frequency with the experimental results.

3.1. UV–Vis absorption spectra and FMO study

The UV–Vis spectrum of $[Cu(dmpd)Cl_2]$ has been examined in EtOH using the td-b3lyp/lanl2dz basis set (Fig. 4). The main assignments of the transition bands, the wavelengths, the oscillator strengths and excitation energies are summarized in Table S3. The band assignments are stated using the percentage compositions of the molecular orbitals in the transitions. Fig. 5 shows plots of the isodensity of some boundary molecular orbitals. Using unrestricted calculations, the $[Cu(dmpd)Cl_2]$ complex was optimized with a mixed basis set. Therefore, each of the occupied and virtual (filled and unfilled) molecular orbital appears to be doubled, i.e. alpha-occupied, beta-occupied, alpha-unoccupied and beta-unoccupied orbitals. The UV–Vis experimental spectrum of the copper complex in EtOH showed bands at 258, 230 and 204 nm, whereas the correlated theoretical bands appeared at 264 ($f = 0.007$), 236 ($f = 0.0066$) and 211 ($f = 0.0103$) nm in solution. The TD-DFT results show that the following orbitals H-7(B)->LUMO(B) (97%); H-16(B)->LUMO(B) (18%), H-13(B)->LUMO(B) (48%), HOMO(A)->LUMO(A) (7%); and HOMO(A)->LUMO(A) (85%), HOMO(A)->L + 1(A) (3%), H-13(B)->LUMO(B) (6%), contributed to possible electronic transitions of the copper complex. The contribution of the relevant orbitals to the important electronic transitions is shown in Fig. S3. It was observed that due to a solvent effect, the theoretical bands (λ_{max}) were altered. The electronic and optical properties of the molecules were based on the values of FMO and Eg. Therefore, to get an idea of the electronic properties and optical influence, the distribution patterns of the FMO (Frontier molecular orbital) for the complex were taken into account and the electronic density contours of the complex in the ground state are presented in Fig. 5. An evaluation of the E_{HOMO} and E_{LOMO} energies for the complex is also shown in Fig. 5. The FMOs consists of the HOMO and LUMO, which play a crucial role in accounting for the chemical activity and kinetic stability. The corresponding Eigen values of the energy are applied to develop descriptors of the global reactivity, playing an important role in QSAR development [43]. A large and small gap for the HOMO-LUMO values transmits information about high and low kinetic stability and high and low chemical reactivity, respectively [44]. The energy values of the HOMOs and LUMOs and their energy gap are given in Fig. 5. In the present study, the FMOs are split into HOMOs (alpha and beta) and LUMOs (alpha and beta) due to the geometry optimization of the complex

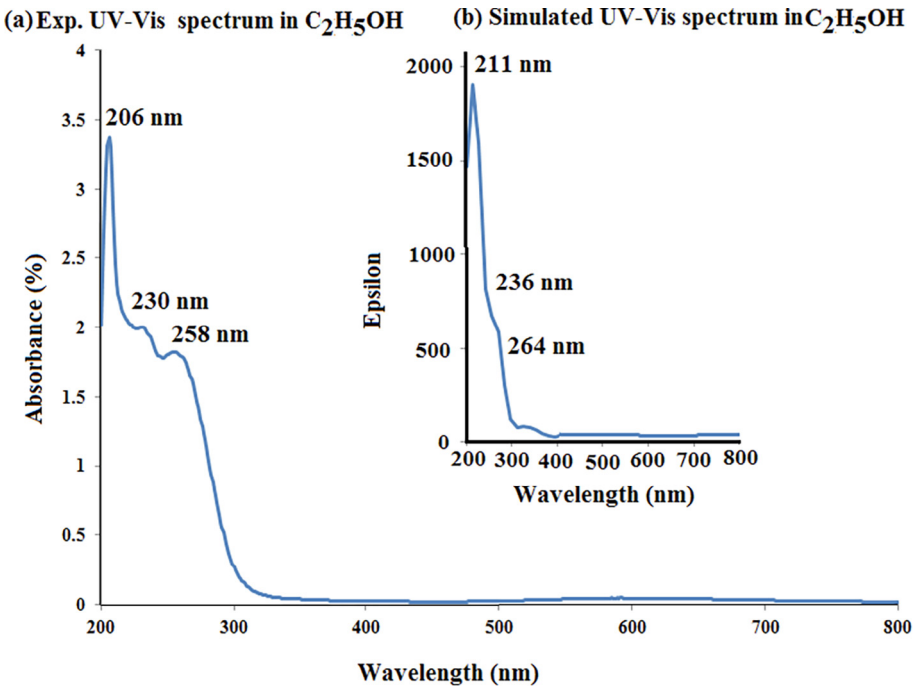

Fig. 4. Experimental and theoretical UV–Vis spectra with the B3LYP/lanl2dz basis set.

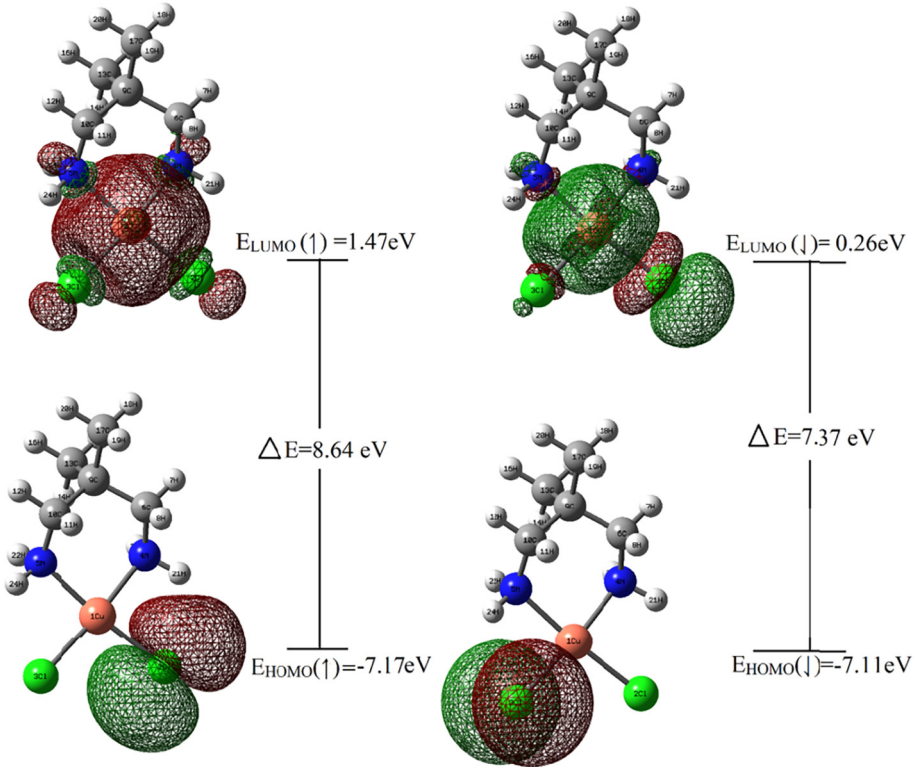

Fig. 5. HOMO–LUMO and their energy gaps between the alpha and beta frontier molecular orbitals of the molecule with B3LYP/6-311G(d,p).

with the b3lyp/6-311G(d,p) basis set in the doublet ground state, and their energy gaps are predicted in each case [Fig. 5]. The alpha-HOMO is almost identical to the beta-HOMO, although the energy of the beta-LUMO is less than that of the alpha-LUMO because the copper orbitals overlap well with ligand orbitals in the β-LUMO. Therefore, the energy gap obtained from alpha HOMO–LUMO is higher than that of beta HOMO–LUMO. From the percentage of the HOMO–LUMO contribution in Table S3, the intramolecular charge transfer properties of the copper complex were demonstrated using group contributions to the molecular

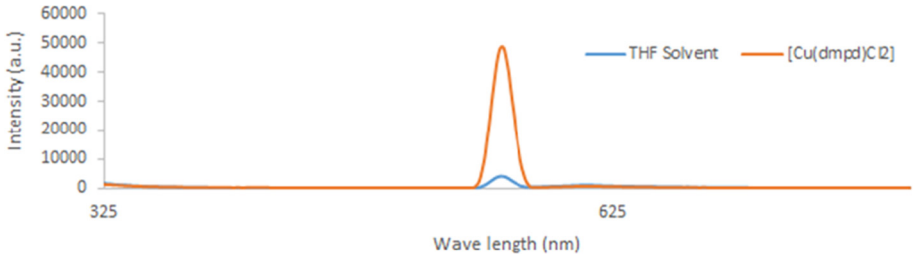

Fig. 6. Emission spectra of the [Cu(dmpd)Cl_2] complex in THF.

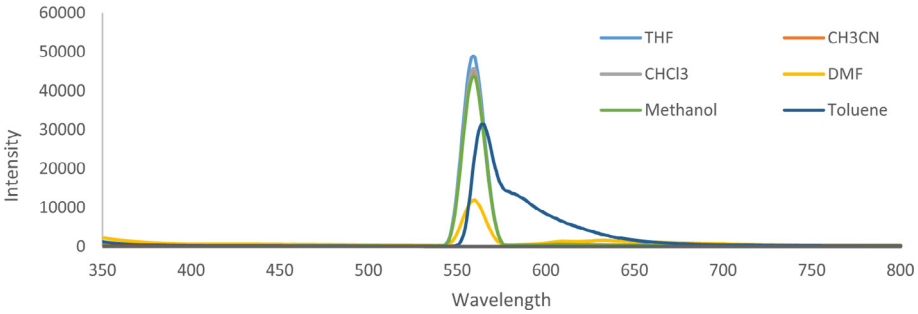

Fig. 7. Sensing behavior of [Cu(dmpd)Cl_2] towards different organic solvents.

orbitals. The high difference in energy (Fig. 5) between these two FMOs (HOMO and LUMO) increases the resistance and stability of the copper complex.

3.2. Other molecular properties

The DFT calculations were used to analyze several properties associated with the molecule, such as the dipole moment, atomic charges, HOMO-LUMO energy eigen values and gaps, thermodynamic parameters and 3D electrostatic molecular potential (MEP) plots for the copper complex. The atomic charges were measured by Mulliken population analysis. The charge values of the atoms are graphically presented in Fig. S5, showing that the copper atom has a high positive charge value. On the other hand, the chlorine and nitrogen atoms show comparatively high negative values. The highly charged N and Cl atoms are directly bound to the Cu atom because of their high electronegativity. All the hydrogen atoms in the complex are found to be positively charged. The 3D graphical plot of the molecular electrostatic potential (MEP) for the copper complex, using B3LYP/6-311G(d,p) with a range of colors from −8.349e−2 (deepest red) to 8.349e−2 (deepest blue), helps to understand the process of biotic recognition and non-bonding interactions (Fig. S6) [45–47]. The MEP plot is also useful in studying electrophilic and nucleophilic chemical reactions. Furthermore, the MEP plot predicts the surface over the chlorine and hydrogen atoms of the nitrogen atoms attached to the copper atoms of the complex as being highly negative and highly positive, respectively. As a result, the red and blue color may be suitable locations for electrophilic and nucleophilic attack, respectively. The green color over some of the metal complex represents the neutral part. Other parameters, such as zero-point vibrational energy, thermodynamic quantity (at 298.15 K), dipole moment, HOMO-LUMO energy eigen values and gap for the complex are given in Table 4S.

The electrochemical behavior of the copper complex was evaluated in water in the presence of KCl as a supporting electrolyte in the range 2 to −1 V. The cyclic voltagram shows an anodic peak at 0.44 V and a cathodic peak at −0.39 V. The current ratio of ipa to ipc was higher than 1, suggesting it to be a quasi-reversible process (Fig. S7).

The photoluminescence behavior of the complex was studied in THF at 280 nm excitation and with a slit width of 5:5. The complex exhibited an intense emission at 558 nm (Fig. 6).

To investigate the effect of solvent on the sensing behavior of the complex towards different small organic molecules, the luminescent behavior of the complex was investigated (Fig. 7). The complex was immersed in various solvents, including THF, $CHCl_3$, CH_3CN, DMF, methanol and toluene. The results clearly show that the florescence emission intensity for the complex was remarkably different for each solvent. However, the florescent emission intensity of the complex was efficiently quenched in the presence of acetone, which was likely due to the interaction of acetone with the complex molecule [48–51].

4. Conclusions

A new ladder type [Cu(dmpd)Cl_2] complex consisting of $CuCl_2$ and 2,2-dimethyl-1,3-diamino propane in 1:1 molar ratio was synthesized and structurally determined. The experimental results were ascertained by computational measurements. The complex exhibited a strong photoluminescence property in tetrahydrofuran and showed an excellent sensing behavior towards a ketone molecule (acetone). Thus, this complex could be a valuable candidate in sensor studies.

Acknowledgments

The authors would like to extend their sincere appreciation to the Deanship of Scientific Research at King Saud University for funding this work through research group project number RG-1436-003. R.K and A.T.K. are thankful to the Ministry of Science and Higher Education and to the Institute of General and Ecological Chemistry, Technical University of Lodz for fund allocations.

Appendix A. Supplementary data

CCDC 1879454 contains the supplementary crystallographic data for [Cu(dmpd)Cl_2]. These data can be obtained free of charge via http://www.ccdc.cam.ac.uk/conts/retrieving.html, or from the Cambridge Crystallographic Data Centre, 12 Union Road, Cambridge CB2 1EZ, UK; fax: (+44) 1223-336-033; or e-mail: deposit@ccdc.cam.ac.uk. Supplementary data to this article can be found online at https://doi.org/10.1016/j.poly.2019.05.053.

References

[1] A.C. Stergiou, S. Papastephanou, C. Tsiamis, Polyhedron 13 (1994) 2285.
[2] N. Masciocchi, M. Moret, A. Sironi, S. Bruni, F. Cariati, A. Pozzi, T. Manfredini, L. Menabue, G.C. Pellacani, Inorg. Chem. 31 (1992) 1401.
[3] D. Moon, C.-S. Lee, J.-H. Choi, J. Chem. Crystallogr. 44 (2014) 306.
[4] D.A. House, Inorg. Chem. 25 (1986) 1671.
[5] S.J. Obrey, S.G. Bott, A.R. Barron, J. Organomet. Chem. 53 (2002) 643.
[6] D. Moon, J.-H. Choi, Spectrochim. Acta, Part A 138 (2015) 774.
[7] L.P. Battaglia, A.B. Corradi, Ledi Menabue, G.C. Pellacani, Dalton Trans. 8 (1981).
[8] I. Warad, A.A. Khan, M. Azam, S.I. AlResayes, S.F. Haddad, J. Mol. Struct. 1062 (2014) 167.
[9] B. Sarkar, M.S. Ray, M.G.B. Drew, A. Figuerola, C. Diaz, A. Ghosh, Polyhedron 25 (2006) 3084.
[10] P. Mukherjee, M.G.B. Drew, A. Ghosh, Eur. J. Inorg. Chem. (2008) 3372.
[11] G.M. Sheldrick, Acta Crystallogr., Sect. A 71 (2015) 3.
[12] G.M. Sheldrick, Acta Crystallogr., Sect. C 71 (2015) 3.
[13] G.M. Sheldrick, Acta Crystallogr., Sect. A 64 (2008) 112.
[14] E. Prince (Ed.), International Tables for Crystallography, Volume C: Mathematical, Physical and Chemical Tables, third ed., Kluwer Academic Publishers, Dordrecht, 2004.
[15] M.J. Frisch, G.W. Trucks, H.B. Schlegel, G.E. Scuseria, M.A. Robb, J.R. Cheeseman, G. Scalmani, V. Barone, B. Mennucci, G.A. Petersson, H. Nakatsuji, M. Caricato, X. Li, H.P. Hratchian, A.F. Izmaylov, J. Bloino, G. Zheng, J.L. Sonnenberg, M. Hada, M. Ehara, K. Toyota, R. Fukuda, J. Hasegawa, M. Ishida, T. Nakajima, Y. Honda, O. Kitao, H. Nakai, T. Vreven, J.A. Montgomery Jr., J.E. Peralta, F. Ogliaro, M. Bearpark, J.J. Heyd, E. Brothers, K.N. Kudin, V.N. Staroverov, R. Kobayashi, J. Normand, K. Raghavachari, A. Rendell, J.C. Burant, S.S. Iyengar, J. Tomasi, M. Cossi, N. Rega, J.M. Millam, M. Klene, J.E. Knox, J.B. Cross, V. Bakken, C. Adamo, J. Jaramillo, R. Gomperts, R.E. Stratmann, O. Yazyev, A.J. Austin, R. Cammi, C. Pomelli, J.W. Ochterski, R.L. Martin, K. Morokuma, V.G. Zakrzewski, G.A. Voth, P. Salvador, J.J. Dannenberg, S. Dapprich, A.D. Daniels, Ö. Farkas, J.B. Foresman, J.V. Ortiz, J. Cioslowski, D.J. Fox, Gaussian 09, revision D.01, Gaussian Inc, Wallingford, CT, 2013.
[16] B.D. Becke, Phys. Rev. A 38 (1988) 3098.
[17] C. Lee, W. Yang, R.G. Parr, Phys. Rev. B 37 (1988) 785.
[18] A. Scha fer, H. Horn, R. Ahlrichs, J. Chem. Phys. 97 (1992) 2571.
[19] P.J. Hay, W.R. Wadt, J. Chem. Phys. 82 (1985) 270.
[20] P.J. Hay, W.R. Wadt, J. Chem. Phys. 82 (1985) 284.
[21] P.J. Hay, W.R. Wadt, J. Chem. Phys. 82 (1985) 299.
[22] N.M. O'Boyle, A.L. Tenderholt, K.M. Langner, J. Comp. Chem. 29 (2008) 839.
[23] A. Wutkowski, C. Nather, W. Bensch, Inorg. Chim. Acta 379 (2011) 16.
[24] D.L. Kepert, Aspects of the stereochemistry of six-coordination, in: S.J. Lippard (Ed.), Progress in Inorganic Chemistry, vol. 23, John Wiley & Sons, Inc., Hoboken, NJ, USA, 1977, pp. 1–65.
[25] W.H. Zachariasen, J. Less Common Met. 62 (1978) 1.
[26] I.D. Brown, Acta Crystallogr., Sect. B 53 (1997) 381.
[27] A. Trzesowska, R. Kruszynski, T.J. Bartczak, Acta Crystallogr., Sect. B 60 (2004) 174.
[28] A. Trzesowska, R. Kruszynski, T.J. Bartczak, Acta Crystallogr., Sect. B 61 (2005) 429.
[29] A. Trzesowska, R. Kruszynski, T.J. Bartczak, Acta Crystallogr., Sect. B 62 (2006) 745.
[30] I.D. Brown, Acta Crystallogr., Sect. B 48 (1992) 553.
[31] L. Sieron, M. Bukowska-Strzyzewska, Acta Crystallogr., Sect. C 55 (1999) 1230.
[32] N.E. Brese, M. O'Keeffe, Acta Crystallogr., Sect. B 47 (1991) 192.
[33] G.R. Desiraju, T. Steiner, The Weak Hydrogen Bond in Structural Chemistry and Biology, Oxford University Press, Oxford, 1999.
[34] J. Bernstein, R.E. Davis, L. Shimoni, N.-L. Chang, Angew. Chem. Int. Ed. Engl. 34 (1995) 1555.
[35] S. Grimme, J. Antony, S. Ehrlich, H. Krieg, J. Chem. Phys. 132 (2010) 154104.
[36] T. Lu, F.W. Chen, J. Mol. Model. 19 (2013) 5387.
[37] F. Biegler-Konig, J. Schonbohm, D. Bayles, J. Comput. Chem. 22 (2001) 545.
[38] Jong-Ha Choi, S.H. Lee, J. Mol. Struct. 932 (2009) 84.
[39] D. Moon, Jong-Ha Choi, Spectrochim. Acta, Part A 138 (2015) 774.
[40] A. Wutkowski, C. Näther, W. Bensch, Inorg. Chim. Acta 379 (2011) 16.
[41] M.K. Assefa, J.L. Devera, A.D. Brathwaite, J.D. Mosley, M.A. Duncan, Chem. Phys. Lett. 640 (2015) 175.
[42] G. Socrates, Infrared Characteristic Group Frequencies, third ed., Wiley Interscience Publications, New York, 1980.
[43] R. Parthasarathi, V. Subramanian, D.R. Roy, P.K. Chattaraj, Bioorg. Med. Chem. 12 (2004) 5533.
[44] Jun-ichi Aihara, J. Phys. Chem. A 103 (1999) 7487.
[45] B. Kosar, C. Albayrak, Spectrochim. Acta, Sect. A 78 (2011) 160.
[46] M.J. Alam, S. Ahmad, Spectrochim. Acta, Sect. A 128 (2014) 653.
[47] M.J. Alam, S. Ahmad, Spectrochim. Acta, Sect. A 96 (2012) 992.
[48] C. Ma, C.Q. Jiao, Z.G. Sun, Y.Y. Zhu, X.W. Zhang, M.L. Wang, D. Yang, Z. Zhao, H. Y. Li, B. Xing, RSC Adv. 5 (2015) 79041.
[49] Y. Deng, Z.Y. Yao, P. Wang, Y. Zhao, Y.S. Kang, W.Y. Sun, Sensor Actuat. B-Chem. 244 (2017) 114.
[50] G. Porter, S.K. Dogra, R.O. Loutfy, S.E. Sugrmori, R.W. Yip, J. Chem. Soc., Faraday Trans. 69 (1973) 1462.
[51] Z.-Q. Liu, Y. Zhao, X.-D. Zhang, Y.-S. Kang, Q.-Y. Lu, M. Azam, S.I. Al-Resayes, Wei-Yin Sun, Dalton Trans. 46 (2017) 13943.